Antiferromagnetic domain wall motion driven by spin-orbit torques

Takayuki Shiino,[1,*] Se-Hyeok Oh,[2,*] Paul M. Haney,[3] Seo-Won Lee,[4]
Gyungchoon Go,[4] Byong-Guk Park,[1,†] and Kyung-Jin Lee[2,4,5,‡]

[1]*Department of Materials Science and Engineering, KAIST, Daejeon 34141, Korea*
[2]*Department of Nano-Semiconductor and Engineering, Korea University, Seoul 02841, Korea*
[3]*Center for Nanoscale Science and Technology, National Institute of Standards and Technology, Gaithersburg, Maryland 20899-6202, USA*
[4]*Department of Materials Science and Engineering, Korea University, Seoul 02841, Korea*
[5]*KU-KIST Graduate School of Converging Science and Technology, Korea University, Seoul 02841, Korea*

(Dated: July 20, 2016)

We theoretically investigate dynamics of antiferromagnetic domain walls driven by spin-orbit torques in antiferromagnet/heavy metal bilayers. We show that spin-orbit torques drive antiferromagnetic domain walls much faster than ferromagnetic domain walls. As the domain wall velocity approaches the maximum spin-wave group velocity, the domain wall undergoes Lorentz contraction and emits spin-waves in the terahertz frequency range. The interplay between spin-orbit torques and the relativistic dynamics of antiferromagnetic domain walls leads to the efficient manipulation of antiferromagnetic spin textures and paves the way for the generation of high frequency signals from antiferromagnets.

PACS numbers: 85.75.-d; 75.50.Ee; 75.78.Fg; 75.70.Tj

Antiferromagnets are ordered spin systems in which the magnetic moments are compensated on an atomic scale. The antiferromagnetic order and consequent zero net magnetic moment are maintained by antiferromagnetic exchange coupling of neighboring spins. Any external disturbance competes directly with the large antiferromagnetic exchange, which results in magnetic excitations in terahertz frequency ranges [1]. Furthermore, an antiferromagnet has no magnetic stray field, which is beneficial for integrated circuits because the stray field is a primary source of detrimental magnetic perturbations [2, 3]. These attractive features of antiferromagnets have led to the recent development of *antiferromagnetic spintronics*, an emerging research field which pursues the use of antiferromagnets as active elements in spintronic-based devices [4].

The principal discipline of antiferromagnetic spintronics is the robust detection and manipulation of the antiferromagnetic order. The antiferromagnetic order can be electrically probed through the (tunneling) anisotropic magnetoresistance effect [5] or the spin pumping effect [6, 7]. Significant progress has also been made on the manipulation of the antiferromagnetic order using both charge and spin currents [8]. Conventional spin-transfer torque enables current-driven manipulation of antiferromagnetic spin textures such as antiferromagnetic domain walls [9–11] and antiferromagnetic skyrmions [12, 13]. We note however that most previous studies on current-driven manipulation of antiferromagnetic order have neglected spin-orbit coupling.

The influence of spin-orbit coupling on spin transport and magnetization dynamics has recently attracted considerable attention, as it enables the study of fundamental interactions among conduction electron spin, electron orbit, and local magnetization. In ferromagnet/heavy metal bilayers, an in-plane current generates spin-orbit spin-transfer torques (SOTs) [14, 15]. The microscopic origin of these torques remains under debate, but they can be classified according to their direction. In the coordinate system of Fig. 1, the "field-like" torque induces precession of spins around the y-axis, while the "damping-like" torque directs the spin towards the y-axis. Spin-orbit coupling additionally induces a noncollinear magnetic exchange in these bilayer systems known as the interfacial Dzyaloshinskii-Moriya interaction (DMI), which stabilizes Néel domain walls in ferromagnets. The SOT combined with DMI efficiently drives a ferromagnetic domain wall [16, 17]. Recently, current-driven relativistic Néel-order fields in antiferromagnets [18] and consequent domain wall motion [19] have been predicted theoretically and SOT switching of antiferromagnetic order has been confirmed experimentally [20], indicating the relevance of SOT in antiferromagnets with inversion asymmetry. This relativistic Néel-order field is present in only a specific class of antiferromagnets for which the spin sublattices of the antiferromagnet individually break inversion symmetry, but form inversion partners with each other.

In this Letter, we investigate SOT-driven antiferromagnetic domain wall motion in antiferromagnet/heavy metal bilayers in the presence of interfacial DMI, based on the collective coordinate approach [9–11] and atomistic spin model simulations [21]. Because SOTs in antiferromagnet/heavy metal bilayers emerge by the *structural inversion asymmetry*, our result is applicable to a wide variety of antiferromagnets in contact with a heavy metal layer. We show that at reasonable current densities the antiferromagnetic domain wall velocity can reach

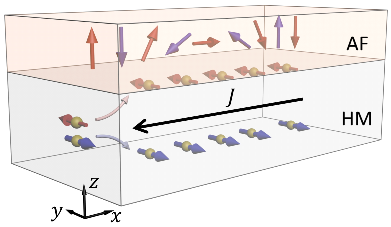

FIG. 1: Schematic illustration of an antiferromagnet (AF)/heavy metal (HM) bilayer system. An in-plane charge current J generates a perpendicular spin current, which in turn generates SOTs acting on antiferromagnetic moments.

a few kilometers per second, which is much larger than that of a ferromagnetic domain wall. As the wall velocity approaches the maximum group velocity of spin-waves, it undergoes Lorentz contraction and emits spin-waves with wavelength on the order of the material lattice constant. The frequency of emitted spin waves is in the terahertz range and thus the antiferromagnetic domain wall can be used as a direct-current-driven terahertz source.

We consider an antiferromagnetic domain wall in a one-dimensional nanowire system composed of an antiferromagnet/heavy metal bilayer with perpendicular magnetic anisotropy (Fig. 1). We note that our result is also applicable to in-plane anisotropy [22]. An in-plane current flowing along the x-axis generates field-like and damping-like SOTs [15]. For the analytical description, we use the nonlinear sigma model in the continuum approximation [10]. To begin, we define the total and staggered magnetization as follows: $\mathbf{m} \equiv \mathbf{m}_1(x,t) + \mathbf{m}_2(x,t)$ and $\mathbf{l} \equiv \mathbf{m}_1(x,t) - \mathbf{m}_2(x,t)$ where $\mathbf{m}_1(x,t)$ and $\mathbf{m}_2(x,t)$ are respectively the magnetic moment densities of two sub-lattices with $|\mathbf{m}_1(x,t)| = |\mathbf{m}_2(x,t)| = m_s$. In the following, we discuss the antiferromagnetic domain wall dynamics with $\mathbf{m}(x,t)$ and $\mathbf{n}(x,t)(\equiv \mathbf{l}(x,t)/l)$ and expand equations up to second order in small parameters [9], assuming that time-, space-derivative, damping, SOTs, anisotropy, and interfacial DMI are small.

The leading-order free energy in the continuum approximation is

$$U = \int \Big[\frac{a}{2}|\mathbf{m}|^2 + \frac{A}{2}(\frac{\partial \mathbf{n}}{\partial x})^2 + L\mathbf{m}\cdot\frac{\partial \mathbf{n}}{\partial x} - \frac{K}{2}(\mathbf{e}_z\cdot\mathbf{n})^2 + \frac{D}{2}\mathbf{e}_y\cdot(\mathbf{n}\times\frac{\partial \mathbf{n}}{\partial x})\Big]d\mathbf{r}, \quad (1)$$

where a and A are the homogeneous and inhomogeneous exchange constants, respectively, L is the parity-breaking exchange constant [23, 24], and K and D denote the easy-axis anisotropy and interfacial DMI, respectively. From the functional derivative of the energy density, we obtain effective fields to lowerst order $\mathbf{f}_\mathrm{m} = -\frac{\delta U}{\delta \mathbf{m}}$ and $\mathbf{f}_\mathrm{n} = -\frac{\delta U}{\delta \mathbf{n}}$.

Disregarding nonlinear terms, the equations of motion are:

$$\frac{\partial \mathbf{n}}{\partial t} = (\gamma \mathbf{f}_\mathrm{m} - G_1\frac{\partial \mathbf{m}}{\partial t})\times\mathbf{n} + \mathbf{T}^\mathrm{n}_\mathrm{SOT}, \quad (2)$$

$$\frac{\partial \mathbf{m}}{\partial t} = (\gamma \mathbf{f}_\mathrm{n} - G_2\frac{\partial \mathbf{n}}{\partial t})\times\mathbf{n} + \mathbf{T}^\mathrm{m}_\mathrm{SOT}, \quad (3)$$

where γ is the gyromagnetic ratio, and G_1 and G_2 are damping parameters [10, 11]. Rewriting the field-like and damping-like torques in terms of $\mathbf{n}$ and $\mathbf{m}$ and retaining lowest order terms leads to: $\mathbf{T}^\mathrm{n}_\mathrm{SOT} = \frac{\gamma B_\mathrm{D}}{l}\mathbf{n}\times(\mathbf{m}\times\mathbf{e}_y) + \gamma B_\mathrm{F}\mathbf{n}\times\mathbf{e}_y$ and $\mathbf{T}^\mathrm{m}_\mathrm{SOT} = \gamma B_\mathrm{D} l\mathbf{n}\times(\mathbf{n}\times\mathbf{e}_y) + \gamma B_\mathrm{F}\mathbf{m}\times\mathbf{e}_y$ [6] where $B_\mathrm{D}(= \mu_\mathrm{B}\theta_\mathrm{SH}J/\gamma e m_s t_z)$ and $B_\mathrm{F}(= \chi B_\mathrm{D})$ denote effective fields corresponding to the damping-like and field-like components of SOT, respectively, t_z is the thickness of antiferromagnet, θ_SH is the effective spin Hall angle, μ_B is the Bohr magneton, e is the electron charge, J is the current density, and χ is the ratio of B_F to B_D.

We introduce the collective coordinates for the domain wall position r and angle ϕ, and the ansatz for the wall profile [25]: $\mathbf{n}(x,t) = (\sin\theta\cos\phi, \sin\theta\sin\phi, \cos\theta)$ where $\theta = 2\tan^{-1}[\exp(\frac{x-r}{\lambda})]$, and λ is the domain wall width. Following the procedure in Ref. [11], $\mathbf{m}$ can be expressed in terms of $\mathbf{n}$ by combining Eqs. (2) and (3). Substituting the wall profile into $\mathbf{n}$ and keeping leading order terms, we obtain the following equations:

$$\ddot{r} + a\gamma G_2\dot{r} + \frac{\pi}{2}a\gamma^2 l\lambda B_\mathrm{D}\cos\phi + \frac{\pi}{2}\gamma\lambda B_\mathrm{F}\dot{\phi}\sin\phi = 0, \quad (4)$$

$$\ddot{\phi} + a\gamma G_2\dot{\phi} - \frac{\pi}{4}\frac{a\gamma^2}{\lambda}D\sin\phi - \frac{\pi}{2}\frac{\gamma}{\lambda}B_\mathrm{F}\dot{r}\sin\phi = 0. \quad (5)$$

We first consider the case for a Néel wall (i.e., $\phi(t=0) = 0$ or π), which is stabilized by nonzero D since the hard-axis anisotropy of antiferromagnetic domain wall is negligible. In Eqs. (4) and (5), all terms having $\sin\phi$ are zero at $t = 0$. With $\dot{r} = 0$ and $\dot{\phi} = 0$ at $t = 0$ (i.e., the domain wall is at rest at $t = 0$), $\dot{\phi}$ is always zero and the steady-state velocity v_DW of Néel wall is given as

$$v_\mathrm{DW} = v_\mathrm{AF} = -\pi\gamma\lambda B_\mathrm{D}/2\alpha, \quad (6)$$

where α $(= G_2/l)$ is the Gilbert damping. It is worthwhile comparing v_AF to the velocity v_F of a Néel type ferromagnetic domain wall driven by SOT [16]:

$$v_\mathrm{F} = \frac{\gamma\pi D}{2m_s\sqrt{1+(\alpha D/B_\mathrm{D} m_s\lambda)^2}}. \quad (7)$$

In the small B_D limit, $|v_\mathrm{F}| = |v_\mathrm{AF}|$. This equivalence is however broken when B_D is large. For a ferromagnetic wall, ϕ increases with B_D so that v_F saturates to $\gamma\pi D/2m_s$. For an antiferromagnetic wall, on the other hand, ϕ does not vary with time and as a result, v_AF increases linearly with B_D (thus J). This unique property of antiferromagnetic Néel wall leads to a large v_AF especially for a small damping α because $v_\mathrm{AF} \propto 1/\alpha$. A small damping is realized in semiconducting or insulating antiferromagnets such as NiO, MnO, FeO, and CoO, where spin scattering is suppressed.

We next consider the case for a Bloch wall (i.e., $\phi(t=0)=\pi/2$ or $3\pi/2$), corresponding to $D=0$. From Eq. (5), $\dot{\phi}$ is always zero because $\dot{r}=0$ and $\dot{\phi}=0$ at $t=0$. Substituting $\dot{\phi}=0$ and $\cos\phi=0$ in Eq. (4), we find $v_{\rm DW}$ of a Bloch wall is zero when it is driven only by the SOT.

To verify the analytical results, we perform numerical calculations with the atomistic Landau-Lifshitz-Gilbert (LLG) equation [21] for an antiferromagnet [see supplementary material [22] for details of the atomistic model]. The symbols in Fig. 2(a) show numerical results of the steady-state $v_{\rm DW}$ as a function of the current density J when $B_{\rm F}=0$. As predicted by Eq. (6), a Bloch wall does not move whereas the Néel wall velocity linearly increases with J in a low current regime. We find however that the Néel wall velocity saturates in a high current regime, in contrast to the prediction of Eq. (6). As explained above, such saturation behavior of $v_{\rm DW}$ is also expected for a ferromagnetic wall when it is driven by combined effects of SOT and DMI [16]. In case of ferromagnetic walls, the saturation of $v_{\rm DW}$ results from the saturation of the domain wall angle ϕ in the high current regime. In case of antiferromagnetic walls, however, ϕ does not change with time [i.e., $\dot{\phi}=0$; see Eq. (5) and Fig. 2(b)] so that the $v_{\rm DW}$ saturation of an antiferromagnetic domain wall results from a completely different origin.

We find that the spin-wave emission from the antiferromagnetic domain wall is the origin of the $v_{\rm DW}$ saturation in the high current regime. A snap-shot configuration of $\mathbf{n}$ shows that the wall moves to the right while emitting spin-waves to the left [Fig. 2(b); see supplementary movie in [22]]. The reason for spin-wave emission is as follows: The damping-like SOT asymmetrically tilts the domains on the right and the left of wall [see inset of Fig. 2(c)]. Because of the asymmetric domain tilting, the rear (i.e., left) of wall has a steeper gradient of $\mathbf{n}$ and thus a higher exchange energy than the front of wall. As the wall moves faster, the wall width λ shrinks more [see Fig. 2(d)]. As λ approaches the lattice constant, the antiferromagnetic domain wall is unable to sustain its energy and starts to emit spin-waves towards its rear (where the gradient is steeper) to release the energy. Therefore, the spin-wave emission serves as an additional energy dissipation channel and slows down the wall motion.

These interesting dynamics of antiferromagnetic domain walls in the high current regime are a manifestation of the relativistic kinematics originating from the Lorentz invariance of the magnon dispersion [29, 30]. In special relativity, as the velocity of a massive particle approaches the speed of light c, it shrinks via Lorentz contraction and its velocity saturates to c. For the dynamics of antiferromagnets, the speed of light is replaced by the maximum spin-wave group velocity because the antiferromagnetic domain wall can be decomposed into spin-waves and has a finite inertial mass [30]. The velocity limit of an antiferromagnetic domain wall can therefore be described by the relativistic kinematics: it undergoes Lorentz contraction

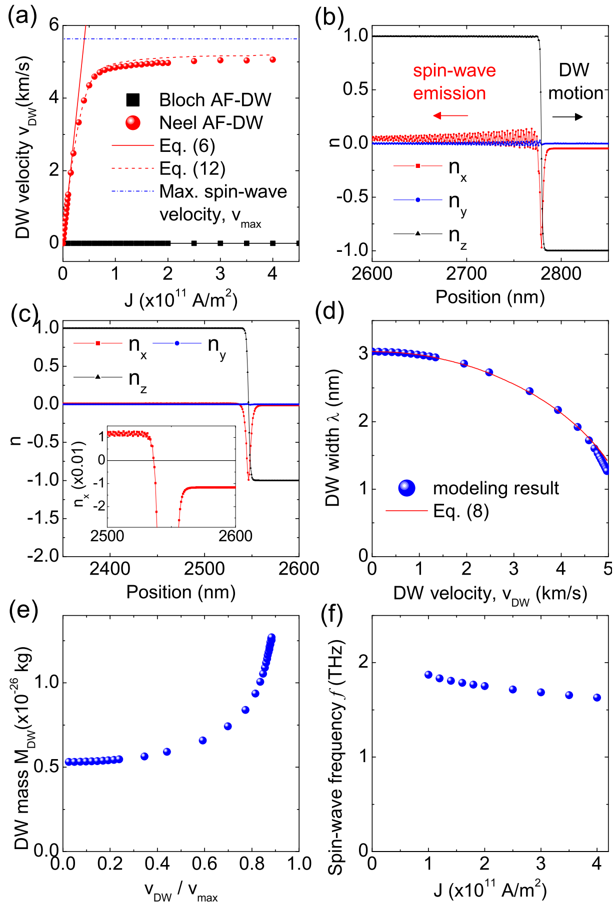

FIG. 2: SOT-driven antiferromagnetic domain wall motion for $B_{\rm F}=0$: (a) Domain wall velocity $v_{\rm DW}$ vs current density J [28]. (b) Configuration of Néel-type antiferromagnetic domain wall at $J=2.0\times10^{11}\,{\rm A/m^2}$. (c) Configuration of Néel-type antiferromagnetic domain wall at $J=0.5\times10^{11}\,{\rm A/m^2}$. Inset shows n_x component. (d) Domain wall width λ vs domain wall velocity $v_{\rm DW}$. (e) Domain wall mass $M_{\rm DW}$ vs $v_{\rm DW}/v_{\rm max}$ where $v_{\rm max}$ is the maximum group velocity of spin-wave. (f) Spin-wave frequency f vs J. Modeling parameters are [26]: $d=0.4\,{\rm nm}$, $A_{\rm sim}=16.0\,{\rm meV}$, $K_{\rm sim}=0.04\,{\rm meV}$, $\mu=3.45\mu_{\rm B}$, $\theta_{\rm SH}=0.1$, $\alpha=0.001$, and $\chi=0$ (i.e., $B_{\rm F}=0$) or 23 (i.e., $B_{\rm F}\neq0$ [27]). We use $D_{\rm sim}=0$ or $D_{\rm sim}=2.0\,{\rm meV}$, obtaining a Bloch or Néel wall, respectively.

as its velocity approaches the maximum spin-wave group velocity, and its velocity saturates to the maximum spin-wave group velocity. Figure 2(d) shows that numerically obtained λ indeed shrinks as $v_{\rm DW}$ becomes larger. The Lorentz contraction of antiferromagnetic domain wall is described by

$$\lambda=\lambda_{\rm eq}\sqrt{1-(v_{\rm DW}/v_{\rm max})^2}, \tag{8}$$

where $\lambda_{\rm eq}$ is the equilibrium domain wall width and $v_{\rm max}$ is the maximum group velocity of spin-wave. To obtain $v_{\rm max}$, we consider spin-waves in the bulk domain regions for simplicity. Spin-waves are described by the equation of motion for a small transverse component n_x as

$$\frac{\partial^2 n_x}{\partial t^2}=a\gamma^2\tilde{A}\frac{\partial^2 n_x}{\partial x^2}-a\gamma^2 K n_x\pm a\gamma^2 l B_{\rm D}, \tag{9}$$

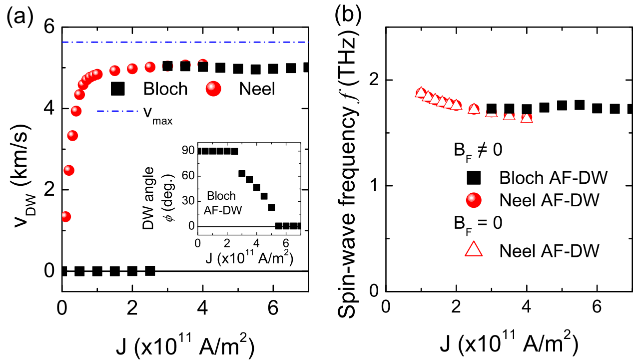

FIG. 3: SOT-driven antiferromagnetic domain wall motion for $B_{\rm F} \neq 0$ ($\chi = 23$ [27]): (a) Domain wall velocity $v_{\rm DW}$ vs current density J [28]. Inset shows the domain wall angle ϕ for an antiferromagnetic domain wall that is initially of Bloch type. (b) Spin-wave frequency f vs J. f for $B_{\rm F} = 0$ is also shown for comparison.

where $\tilde{A} = A - L^2/a$ and the upper (lower) sign corresponds to the up (down) domain. The dispersion relation and corresponding group velocity are given by

$$\omega = \gamma\sqrt{a(\tilde{A}k^2 + K)}, \tag{10}$$

$$v_{\rm g} = \frac{d\omega}{dk} = \frac{\gamma a l d}{2\sqrt{1 + 4K/al^2d^2k^2}}, \tag{11}$$

and thus $v_{\rm max} = \gamma a l d/2$. For the modeling parameters, $v_{\rm max}$ is about 5.6 km/s as shown in Fig. 2(a). With $v_{\rm max}$ given above, the relativistically corrected $v_{\rm DW}$ is given as

$$v_{\rm DW} = \frac{\gamma a l d}{2}\sqrt{1 - (\lambda/\lambda_{\rm eq})^2}. \tag{12}$$

Equations (8) and (12) describe the numerical results reasonably well [see Fig. 2(a) and (d)].

Two remarks on the relativistic kinematics of SOT-driven antiferromagnetic domain wall motion are in order. Firstly, it is also associated with the inertial mass of the wall. In steady-state motion, the effective inertial mass $M_{\rm DW}$ of antiferromagnetic domain wall is $M_{\rm DW} = 2\rho w t_z/\lambda = 2\rho w t_z/\lambda_{\rm eq}\sqrt{1-(v_{\rm DW}/v_{\rm max})^2}$ where w is the wire width. Because of the Lorentz contraction, $M_{\rm DW}$ increases by the Lorentz factor $1/\sqrt{1-(v_{\rm DW}/v_{\rm max})^2}$ as $v_{\rm DW}$ increases (Fig. 2(e)). Secondly, the frequency of emitted spin-waves is in the terahertz range. Using the modeling parameters in the spin-wave dispersion given above, one finds that the spin-wave frequency $f_{\rm max}$ ($=\omega/2\pi$) corresponding to $v_{\rm max}$ is about 2.5 THz. The numerically obtained spin-wave frequency is slightly lower than $f_{\rm max}$ but is still in the terahertz range [Fig. 2(f)]. This suggests that the antiferromagnetic domain wall can be used as a terahertz source of electric signal. The power of THz signal estimated based on the spin pumping and inverse spin-Hall effect [6, 7] is of the order of μW [22], which is measurable.

We next show numerical results for $B_{\rm F} \neq 0$ (Fig. 3). $B_{\rm F}$ does not affect dynamics of the Néel wall: $v_{\rm DW}$ of the Néel wall is almost independent of $B_{\rm F}$. On the other hand, $B_{\rm F}$ affects dynamics of Bloch wall substantially. For $B_{\rm F} = 0$ the Bloch wall does not move [Fig. 2(a)] whereas for $B_{\rm F} \neq 0$ it moves with $v_{\rm DW} \approx v_{\rm max}$ above a certain threshold current density [$J_{\rm th} = 2.5 \times 10^{11}$ A/m^2; see Fig. 3(a)]. This fast motion of the Bloch wall is accompanied by a current-dependent change in the domain wall angle ϕ [inset of Fig. 3(a)], because a nonzero $B_{\rm F}$ transforms an initial Bloch wall into a Néel type wall. This transformation is known as the *spin-flop* transition of an antiferromagnet [32]. When an antiferromagnet is subject to a large magnetic field applied along the staggered magnetization $\mathbf{n}$, the spin sublattice antiparallel to the applied field is energetically unfavorable. At a threshold field, the spins *flop* to a configuration where both sublattices are perpendicular to the applied field [33], which corresponds to the transformation from a Bloch to a Néel wall. From Fig. 3(a), we find that $v_{\rm DW}$ saturates in the high current regime as in the case with $B_{\rm F} = 0$. This $v_{\rm DW}$ saturation also originates from the emission of spin-waves in the terahertz frequency ranges [Fig. 3(b)].

In summary, the SOT can efficiently move the antiferromagnetic domain wall. The damping-like SOT is the main driving force whereas the field-like SOT is effective by transforming a Bloch wall into a Néel wall. The antiferromagnetic domain wall velocity can reach a few kilometers per second, which is orders of magnitude larger than the ferromagnetic domain wall velocity. The relativistic kinematics of antiferromagnets results in the saturation of $v_{\rm DW}$ in the high current regime, which is accompanied by the emission of spin-waves with frequency in the terahertz range. An antiferromagnetic domain wall can therefore serve as a terahertz source.

We end this paper with two remarks. Firstly, the relativistic kinematics is not unique to antiferromagnetic domain walls: a ferromagnetic domain wall can exhibit relativistic motion in systems with biaxial anisotropy, which is essential for a finite inertial mass. Wang *et al.* [34] reported field-driven ferromagnetic domain wall motion with spin-wave emission. This relativistic motion is however realized only by assuming very large hard-axis anisotropy, comparable to exchange energy. This unrealistic assumption is required to push the wall width to a few lattice constants. In contrast, for antiferromagnetic domain walls, the condition of a-few-lattice-constant wall width is naturally realized by the SOT. Secondly, Yang *et al.* [35] reported a very high $v_{\rm DW}$($\approx$ 750 m/s^{-1}) in synthetic antiferromagnets. Even though synthetic antiferromagnets share some of the attractive properties of antiferromagnetic devices, e.g. absence of stray magnetic fields and high domain wall velocity, we find that THz spin-wave emission may be not possible for synthetic antiferromagnets with a reasonable antiferromagnetic RKKY interaction because the RKKY interaction is insufficient to suppress the domain wall angle tilting [22].

We acknowledge fruitful discussions with T. Ono, A.

Manchon, J. Xiao, R. Cheng, S. K. Kim, O. Tchernyshyov, O. A. Tretiakov, K.-W. Kim, and M. D. Stiles. This work was supported by the National Research Foundation of Korea (NRF) (2015M3D1A1070465, 2011-0027905, NRF-2014R1A2A1A11051344).

---

* These two authors contributed equally to this work.
† Electronic address: `bgpark@kaist.ac.kr`
‡ Electronic address: `kj_lee@korea.ac.kr`

[1] T. Kampfrath, A. Sell, G. Klatt, A. Pashkin, S. Mährlein, T. Dekorsy, M. Wolf, M. Fiebig, A. Leitenstorfer, and R. Huber, Nat. Photon. **5**, 31 (2011).
[2] A. H. MacDonald and M. Tsoi, Phil. Trans. R. Soc. A **369**, 3098 (2011).
[3] R. Duine, Nat. Mater. **10**, 344 (2011).
[4] T. Jungwirth, X. Marti, P. Wadley, and J. Wunderlich, Nat. Nanotechnol. **11**, 231 (2016).
[5] B. G. Park, J. Wunderlich, X. Martí, V. Holý, Y. Kurosaki, M. Yamada, H. Yamamoto, A. Nishide, J. Hayakawa, H. Takahashi, A. B. Shick, and T. Jungwirth, Nat. Mater. **10**, 347 (2011); Y. Y. Wang, C. Song, B. Cui, G. Y. Wang, F. Zeng, and F. Pan, Phys. Rev. Lett. **109**, 137201 (2012); X. Marti, I. Fina, C. Frontera, J. Liu, P. Wadley, Q. He, R. J. Paull, J. D. Clarkson, J. Kudrnovský, I. Turek, J.Kuneš, D. Yi, J.-H. Chu, C. T. Nelson, L. You, E. Arenholz, S. Salahuddin, J. Fontcuberta, T. Jungwirth, and R. Ramesh, Nat. Mater. **13**, 367 (2014); T. Moriyama, N. Matsuzaki, K.-J. Kim, I. Suzuki, T. Taniyama, and T. Ono, Appl. Phys. Lett. **107**, 122403 (2015).
[6] R. Cheng, J. Xiao, Q. Niu, and A. Brataas, Phys. Rev. Lett. **113**, 057601 (2014).
[7] R. Cheng, D. Xiao, and A. Brataas, Phys. Rev. Lett. **116**, 207603 (2016).
[8] A. S. Núñez, R. A. Duine, P. Haney, and A. H. MacDonald, Phys. Rev. B **73**, 214426 (2006); Z. Wei, A. Sharma, A. S. Núñez, P. M. Haney, R. A. Duine, J. Bass, A. H. MacDonald, and M. Tsoi, Phys. Rev. Lett. **98**, 116603 (2007); S. Urazhdin and N. Anthony, Phys. Rev. Lett. **99**, 046602 (2007); P. M. Haney and A. H. MacDonald, Phys. Rev. Lett. **100**, 196801 (2008).
[9] A. C. Swaving and R. A. Duine, Phys. Rev. B **83**, 054428 (2011).
[10] K. M. D. Hals, Y. Tserkovnyak, A. Brataas, Phys. Rev. Lett. **106**, 107206 (2011).
[11] E. G. Tveten, A. Qaiumzadeh, O. A. Tretiakov, and A. Brataas, Phys. Rev. Lett. **110**, 127208 (2013).
[12] X. Zhang, Y. Zhou, and M. Ezawa, Sci. Rep. **6**, 24795 (2016).
[13] J. Barker and O. A. Tretiakov, Phys. Rev. Lett. **116**, 147203 (2016).
[14] I. M. Miron, K. Garello, G. Gaudin, P.-J. Zermatten, M. V. Costache, S. Auffret, S. Bandiera, B. Rodmacq, A. Schuhl, and P. Gambadella, Nature (London) **476**, 189 (2011); L. Liu, C.-F. Pai, Y. Li, H. W. Tseng, D. C. Ralph, and R. A. Buhrman, Science **336**, 555 (2012).
[15] K. Obata and G. Tatara, Phys Rev. B **77**, 214429 (2008); A. Manchon and S. Zhang, Phys. Rev. B **78**, 212405 (2008); A. Matos-Abiague and R. L. Rodriguez-Suarez, Phys. Rev. B **80**, 094424 (2009); X. Wang and A. Manchon, Phys. Rev. Lett. **108**, 117201 (2012); K.-W. Kim, S.-M. Seo, J. Ryu, K.-J. Lee, and H.-W. Lee, Phys. Rev. B **85**, 180404(R) (2012); D. A. Pesin and A. H. MacDonald, Phys. Rev. B **86**, 014416 (2012); E. van der Bijl and R. A. Duine,Phys. Rev. B **86**, 094406 (2012); P. M. Haney, H.-W. Lee, K.-J. Lee, A. Manchon, and M. D. Stiles, Phys. Rev. B **87**, 174411 (2013).
[16] A. Thiaville, S. Rohart, É. Jué, V. Cros, and A. Fert, Europhys. Lett. **100**, 57002 (2012).
[17] S. Emori, U. Bauer, S.-M. Ahn, E. Martinez, and G. S. D. Beach, Nat. Mater. **12**, 611 (2013); K.-S. Ryu, L. Thomas, S.-H. Yang, and S. S. P. Parkin, Nat. Nanotechnol. **8**, 527 (2013).
[18] J. Železný, H. Gao, K. Výborný, J. Zemen, J. Mašek, A. Manchon, J. Wunderlich, J. Sinova, and T. Jungwirth, Phys. Rev. Lett. **113**, 157201 (2014).
[19] O. Gomonay, T. Jungwirth, and J. Sinova, Phys. Rev. Lett. **117**, 017202 (2016).
[20] P. Wadley, B. Howells, J. Zelezny, C. Andrews, V. Hills, R. P. Campion, V. Novak, K. Olejník, F. Maccherozzi, S. S. Dhesi, S. Y. Martin, T. Wagner, J. Wunderlich, F. Freimuth, Y. Mokrousov, J. Kunes, J. S. Chauhan, M. J. Grzybowski, A. W. Rushforth, K. W. Edmonds, B. L. Gal- lagher, and T. Jungwirth, Science **351**, 587 (2016).
[21] R. F. Evans, W. J. Fan, P. Chureemart, T. A. Ostler, M. O. Ellis, and R. W. Chantrell, J. Phys.: Condens. Matter **26**, 103202 (2014).
[22] See supplementary materials.
[23] N. Papanicolaou, Phys. Rev. B. **51**, 15062 (1995).
[24] E. G. Tveten, T. Müller, J. Linder, and A. Brataas, Phys. Rev. B. **93**, 104408 (2016).
[25] L. D. Landau and E. M. Lifshitz, *Electrodynamics of Continuous Media*, Course of Theoretical Physics Vol. 8 (Pergamon, Oxford, 1960).
[26] T. Archer, C. D. Pemmaraju, S. Sanvito, C. Franchini, J. He, A. Filippetti, P. Delugas, D. Puggioni, V. Fiorentini, R. Tiwari, and P. Majumdar, Phys. Rev. B **84**, 115114 (2011).
[27] H. B. M. Saidaoui, A. Manchon, and X. Waintal, Phys. Rev. B **89**, 174430 (2014).
[28] For a monolayer antiferromagnet, the initial Néel antiferromagnetic domain wall is broken when $J > 4 \times 10^{11}\,\mathrm{A/m^2}$. The threshold current density to break the domain wall structure increases with the number of monolayers (not shown). The main conclusion of this work is not altered for multiple monolayers.
[29] F. D. M. Haldane, Phys. Rev. Lett. **50**, 1153 (1983).
[30] S. K. Kim, Y. Tserkovnyak, and O. Tchernyshyov, Phys. Rev. B. **90**, 104406 (2014).
[31] E. G. Tveten, A. Qaiumzadeh, and A. Brataas, Phys. Rev. Lett. **112**, 147204 (2014).
[32] A. H. Morrish, *The Physical Principles of Magnetism* (Wiley, New York, 1965).
[33] J. Nogués, L. Morellon, C. Leighton, M. R. Ibarra, and I. K. Schuller, Phys. Rev. B. **61**, R6455 (2000).
[34] X. S. Wang and X. R. Wang, Phys. Rev. B. **90**, 184415 (2014).
[35] S.-H. Yang, K.-S. Ryu, and S. Parkin, Nat. Nanotechnol. **10**, 221 (2015).

Supplementary Material for "Antiferromagnetic domain wall motion driven by spin-orbit torques"

Takayuki Shiino,[1,*] Se-Hyeok Oh,[2,*] Paul M. Haney,[3] Seo-Won Lee,[4]
Gyungchoon Go,[4] Byong-Guk Park,[1,†] and Kyung-Jin Lee[2,4,5,‡]

[1]*Department of Materials Science and Engineering, KAIST, Daejeon 34141, Republic of Korea*
[2]*Department of Nano-Semiconductor and Engineering, Korea University, Seoul 02841, Korea*
[3]*Center for Nanoscale Science and Technology, National Institute of Standards and Technology, Gaithersburg, Maryland 20899-6202, USA*
[4]*Department of Materials Science and Engineering, Korea University, Seoul 02841, Korea*
[5]*KU-KIST Graduate School of Converging Science and Technology, Korea University, Seoul 02841, Korea*

1. ATOMISTIC MODEL FOR NUMERICAL CALCULATIONS

The Hamiltonian of the antiferromagnets is

$$\mathcal{H} = A_{\rm sim}\sum_i \mathbf{S}_i\cdot\mathbf{S}_{i+1} - K_{\rm sim}\sum_i(\mathbf{S}_i\cdot\mathbf{e}_{\rm z})^2 - D_{\rm sim}\sum_i \mathbf{e}_y\cdot(\mathbf{S}_i\times\mathbf{S}_{i+1}) + \frac{\mu_0}{8\pi}m_{\rm s}\mu\sum_{i,j}\left(\mathbf{S}_i\cdot\mathbf{S}_j - \frac{3(\mathbf{S}_i\cdot\mathbf{r}_{ij})(\mathbf{S}_j\cdot\mathbf{r}_{ij})}{r^2}\right), \quad (1)$$

where $\mathbf{S}_i$ represents the normalized magnetic moment (i.e., $|\mathbf{S}_i| = 1$) at lattice site i, μ is the magnetic moment per lattice site, and $A_{\rm sim}, K_{\rm sim}, D_{\rm sim}$ denote the exchange, anisotropy, and DMI energies, respectively. The last term represents the dipole-dipole interaction where $\mathbf{r}_{ij}$ is a distance vector between lattice sites i and j (i.e., $|\mathbf{r}_{ij}| = r$). The atomistic LLG equation including spin-orbit torques is as follows:

$$\frac{\partial\mathbf{S}_i}{\partial t} = -\gamma\mathbf{S}_i\times\mathbf{B}_{\rm eff} + \alpha\mathbf{S}_i\times\frac{\partial\mathbf{S}_i}{\partial t} + \gamma B_{\rm D}\mathbf{S}_i\times(\mathbf{S}_i\times\mathbf{e}_y) + \gamma B_{\rm F}(\mathbf{S}_i\times\mathbf{e}_y), \quad (2)$$

where $\mathbf{B}_{\rm eff} = -\frac{1}{\mu}\frac{\delta\mathcal{H}}{\delta\mathbf{S}_i}$ is the effective field.

2. RELATIVISTIC DOMAIN WALL DYNAMICS IN ANTIFERROMAGNETS WITH IN-PLANE MAGNETIC ANISOTROPY

In this section, we investigate SOT-driven domain wall motion in antiferromagnets with in-plane magnetic anisotropy (IMA). We introduce the collective coordinates for the domain wall position r and angle ϕ, and Walker ansatz for IMA domain wall profile expressed in the staggered vector: $n(x,t) = (n_x, n_y, n_z) = (\cos\theta, \sin\theta\cos\phi, \sin\theta\sin\phi)$ where $\theta = 2\tan^{-1}[\exp(\frac{x-r}{\lambda})]$ and λ is the domain wall width. In this case, ϕ is defined within the $y-z$ plane. With DMI ($D \neq 0$), ϕ is $\pi/2$ or $3\pi/2$, and without DMI ($D = 0$), ϕ is 0 or π. In the same manner as the case with perpendicular magnetic anisotropy (PMA) shown in the main text, we obtain the following equations of motion:

$$\ddot{r} + a\gamma G_2\dot{r} - \frac{\pi a\gamma^2 l\lambda B_D}{2}\sin\phi + \frac{\pi\gamma\lambda B_F}{2}\dot{\phi}\cos\phi = 0, \quad (3)$$

$$\ddot{\phi} + a\gamma G_2\dot{\phi} - \frac{\pi a\gamma^2 D}{4\lambda}\cos\phi - \frac{\pi\gamma B_F}{2\lambda}\dot{r}\cos\phi = 0. \quad (4)$$

We note that these equations of motion are similar to those for PMA domain wall case. Therefore, the steady-state velocity of IMA domain wall is also similar to that of PMA domain wall:

$$v_{\rm DW} = -\frac{\pi\gamma\lambda B_D}{2\alpha}\sin\phi. \quad (5)$$

We perform numerical simulation with atomistic LLG equation for IMA domain wall. In this case, we consider only the damping-like torque ($B_F = 0$) for simplicity. We use modeling parameters as follows: $d = 0.4\,$nm, $A_{\rm sim} = 16.0\,$meV, $K_{\rm sim} = 0.2\,$meV, $\mu = 3.45\mu_{\rm B}$, $\alpha = 0.001$, and $\theta_{\rm SH} = 0.1$. We set $D_{\rm sim} = 0\,$meV for zero DMI case and $D_{\rm sim} = 2.0\,$meV for non-zero DMI case, respectively.

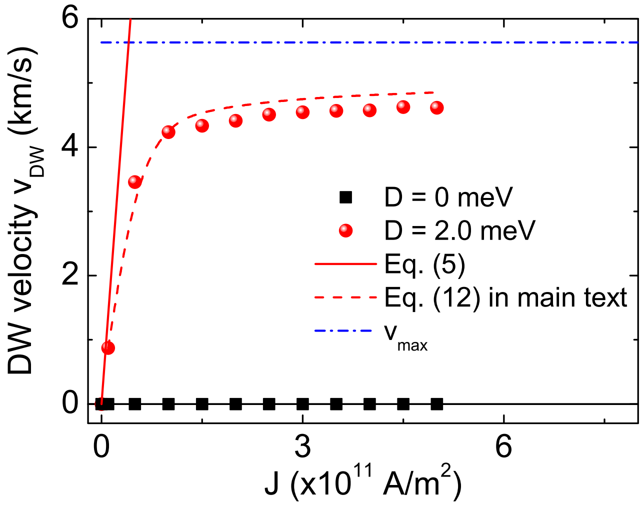

FIG. 1: Steady-state domain wall velocity as a function of current density for in-plane magnetic anisotropy (IMA) case. Symbols correspond to numerical calculations, while solid lines correspond to analytical solutions. Blue dashed line represents the maximum spin-wave group velocity. Domain wall cannot be retained above $J = 5 \times 10^{11}$ A/m^2 for non-zero DMI case.

Figure 1 shows numerical results of steady-state velocity v_{DW} of IMA case as a function of the current density J. For non-zero DMI, v_{DW} saturates to the maximum spin-wave group velocity with emitting THz spin-waves. All these results are analogous with PMA Néel wall case and Eq. (8) in the main text describes the simulation results well. Furthermore, the case of zero DMI is also the same as the case of PMA Bloch wall which does not move by SOT. Therefore, we confirm that the relativistic kinematics of antiferromagnetic domain wall occurs regardless of preferred magnetic easy axis.

3. ESTIMATION OF AC POWER ORIGINATING FROM TERAHERTZ SPIN-WAVES

The power originating from THz spin-waves can be estimated by antiferromagnetic spin-pumping and inverse spin-Hall effect in heavy metal (HM). Cheng *et al.* reported that the magnitude of spin mixing conductance at the interface of non-metal/compensated antiferromagnet is similar to that of non-metal/ferromagnet [1]. Based on Cheng's spin pumping theory, we estimate the power as shown below.

The spin-waves inject spin currents into HM via antiferromagnetic spin pumping. The pumped spin current (density) is [1, 2]

$$\frac{e}{\hbar} J^s_{jz} = \frac{1}{2}\Big\{ g_r \left(\mathbf{m}_1 \times \dot{\mathbf{m}}_1 + \mathbf{m}_2 \times \dot{\mathbf{m}}_2 \right) - g_i (\dot{\mathbf{m}}_1 + \dot{\mathbf{m}}_2) \Big\}_j \tag{6}$$

where the subscript j (z) represents the polarization(flow) direction, $g_r(g_i)$ are real(imaginary) part of the spin-mixing conductance, and $\mathbf{m}_k$ $(k = 1, 2)$ is the unit vector along the magnetization in two spin sublattices. Because g_i is usually small compared to g_r, henceforth, we ignore g_i. Note that we also neglect the staggered spin current which decays within a distance of mean free path in the HM.

The spin current injected into the HM induces the charge current J_i via the inverse spin-Hall effect

$$J_i = \theta_{\mathrm{SH}} \epsilon_{ijk} J^s_{jk}, \qquad \theta_{\mathrm{SH}} = \frac{\sigma_{\mathrm{SH}}}{\sigma}, \tag{7}$$

where $\sigma(\sigma_{\mathrm{SH}})$ is the conductivity(spin Hall conductivity) of HM. Substituting Eq. (4) into Eq. (5), we have

$$J_i = \frac{\hbar}{2e} \theta_{\mathrm{SH}} g_r \epsilon_{ij} \left(\mathbf{m}_1 \times \dot{\mathbf{m}}_1 + \mathbf{m}_2 \times \dot{\mathbf{m}}_2 \right)_j . \tag{8}$$

From the numerical simulation results shown in the main text, we take the ansatz of $\mathbf{m}_1$ and $\mathbf{m}_2$ as

$$\mathbf{m}_1 = \hat{\mathbf{z}} + m_x \sin\omega t\,\hat{\mathbf{x}} + m_y \cos\omega t\,\hat{\mathbf{y}}, \quad \mathbf{m}_2 = -\hat{\mathbf{z}} - m_x \sin(\omega t - \phi)\,\hat{\mathbf{x}} + m_y \cos(\omega t - \phi)\,\hat{\mathbf{y}} \quad (m_y < m_x \ll 1) \tag{9}$$

where ϕ is the phase difference between $\mathbf{m}_1$ and $\mathbf{m}_2$. Keeping linear order terms in m_x and m_y we obtain

$$\mathbf{m}_1 \times \dot{\mathbf{m}}_1 \simeq m_x\omega \cos\omega t\,\hat{\mathbf{y}} + m_y\omega \sin\omega t\,\hat{\mathbf{x}}, \qquad \mathbf{m}_2 \times \dot{\mathbf{m}}_2 \simeq m_x\omega \cos(\omega t - \phi)\,\hat{\mathbf{y}} - m_y\omega \sin(\omega t - \phi)\,\hat{\mathbf{x}}. \tag{10}$$

Using Eqs. (6) and (8), we obtain the induced current (density) as

$$J_x = \frac{\hbar}{2e}\theta_{\mathrm{SH}} g_r m_x \omega \left[\cos\omega t + \cos(\omega t - \phi)\right], \qquad J_y = -\frac{\hbar}{2e}\theta_{\mathrm{SH}} g_r m_y \omega \left[\sin\omega t - \sin(\omega t - \phi)\right]. \tag{11}$$

From the Ohm's law and assuming that the spin-wave has a constant amplitude within the length d corresponding to spin-wave attenuation length (i.e., square wave approximation), we obtain the AC power P along x-direction (domain wall propagation direction)

$$P = \overline{I_x V} = \frac{L_y d^2}{\sigma}\overline{J_x^2} = \frac{\hbar^2}{4e^2}\frac{\theta_{\mathrm{SH}}^2}{\sigma} g_r^2 m_x^2 \omega^2 L_y d^2 (1 + \cos\phi) \tag{12}$$

where the upper bar represents time average and L_y is width of the sample. For the typical set of parameters such as

$$\begin{aligned} &\theta_{\mathrm{SH}} = 0.1, \quad \sigma = 10^7 \Omega^{-1}\mathrm{m}^{-1}, \quad g_r = 5.9 \times 10^{14} \Omega^{-1}\mathrm{m}^{-2}, \\ &m_x = 0.1, \quad \omega = 4\pi \times 10^{12}\mathrm{s}^{-1}, \quad L_y = 100\mathrm{nm}, \quad d = 200\mathrm{nm}, \quad \phi = \frac{\pi}{6}, \end{aligned} \tag{13}$$

we obtain $P \simeq 0.4\mu$W, which is measurable in experiments.

4. COMPARISON TO SOT-DRIVEN DOMAIN WALL DYNAMICS IN SYNTHETIC ANTIFERROMAGETS

Recently, Yang *et al.* reported that SOT drives a domain wall in synthetic antiferromagnets very efficiently ($v_{\mathrm{DW}} \approx$ 750 m/s) [3]. As synthetic antiferromagnets share some of the attractive properties of antiferromagnetic devices, e.g. absence of stray magnetic fields and high domain wall velocity, it is meaningful to check whether or not SOT-driven domain wall motion in synthetic antiferromagnets are able to generate THz spin-waves.

Here we check the possibility by performing numerical simulations for SOT-induced domain wall motion in synthetic antiferromagnets (bottom ferromagnet (d_{FM})/ Ru (d_{Ru}) / top ferromagnet (d_{FM})). The Hamiltonian of each ferromagnetic layer in a synthetic antiferromagnet is

$$\begin{aligned} \mathcal{H} \;=\;& A_{\mathrm{sim}} \sum_i \mathbf{S}_i \cdot \mathbf{S}_{i+1} - K_{\mathrm{sim}} \sum_i (\mathbf{S}_i \cdot \mathbf{e}_z)^2 - D_{\mathrm{sim}} \sum_i \mathbf{e}_y \cdot (\mathbf{S}_i \times \mathbf{S}_{i+1}) \\ &+ \frac{\mu_0}{8\pi} m_s \mu \sum_{i,j} \left(\mathbf{S}_i \cdot \mathbf{S}_j - \frac{3(\mathbf{S}_i \cdot \mathbf{r}_{ij})(\mathbf{S}_j \cdot \mathbf{r}_{ij})}{r^2} \right) - J_{\mathrm{RKKY}} \sum_i \mathbf{S}_i \cdot \mathbf{S}_{i'}, \end{aligned} \tag{14}$$

where $\mathbf{S}_i$ represents the normalized magnetic moment (i.e., $|\mathbf{S}_i| = 1$) at lattice site i, μ is the magnetic moment per lattice site, and $A_{\mathrm{sim}}, K_{\mathrm{sim}}, D_{\mathrm{sim}}$ denote the exchange, anisotropy, and DMI energies, respectively.

We assume the damping-like SOTs with opposite sign are applied to top and bottom ferromagnets so that the SOT drives domain wall motion in the same direction in both ferromagnets. We use modeling parameters as follows: $d_{\mathrm{FM}} = 0.4$ nm, $d_{\mathrm{Ru}} = 0.4$ nm, $A_{\mathrm{sim}} = -0.1$ eV, $K_{\mathrm{sim}} = 0.4$ meV, $D_{\mathrm{sim}} = 10$ meV, $\mu = 6.9\mu_{\mathrm{B}}$, $\theta_{\mathrm{SH}} = 0.1$, and $\alpha = 0.001$ with various Ruderman-Kittel-Kasuya-Yosida (RKKY) exchange coupling constants (J_{RKKY}) of -1.0, -5.0, and -10.0 meV. We note that J_{RKKY} of -1.0 meV corresponds to a reasonable value of RKKY interaction in realistic systems.

Figure 2 shows atomistic model results of the synthetic antiferromagnet. For all values of J_{RKKY} studied, we find that v_{DW} saturates in the high current regime (Fig. 2(a)), just like that of *true* antiferromagnets shown in the main text. For J_{RKKY} of -1.0 and -5.0 meV, we find however that the v_{DW} saturation of synthetic antiferromagnets is not caused by THz spin-wave emission but is entirely caused by the tilt of domain wall angle (Fig. 2(b)). This is in contrast to domain wall dynamics of *true* antiferromagnets. In case of *true* antiferromagnets, the domain wall angle is hardly tilted so that v_{DW} tends to linearly increase with the current. As a result, v_{DW} reaches v_{max} at a certain

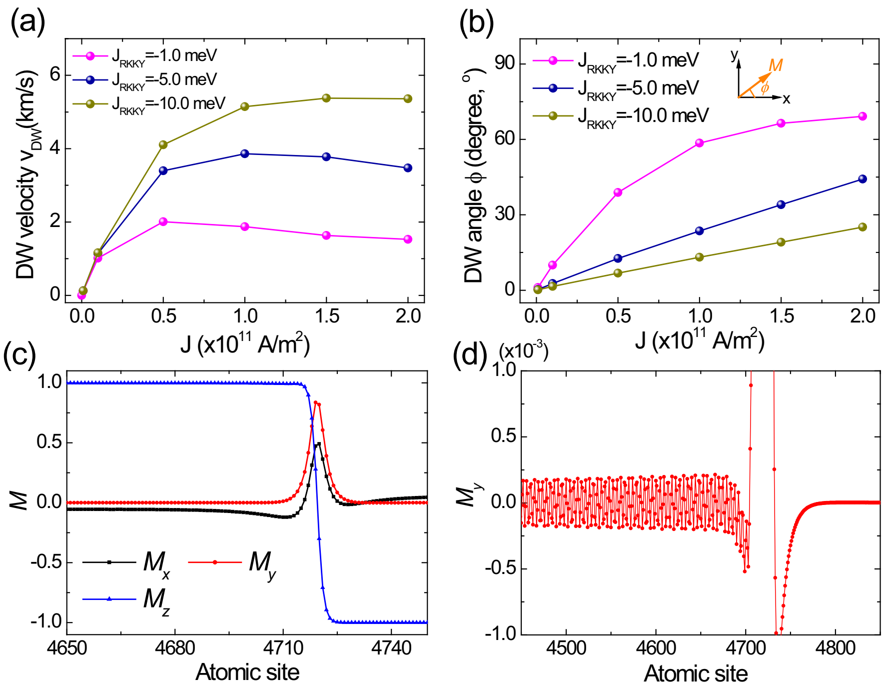

FIG. 2: Atomistic simulation results of a ferromagnetic layer in a synthetic antiferromagnet. We note that the top and bottom ferromagnetic layers are identical so that magnetization dynamics of two layers is also symmetric. (a) steady-state velocity $v_{\rm DW}$ and (b) domain wall angle ϕ as a function of the current density for various $J_{\rm RKKY}$. The angle ϕ is defined as the domain wall angle from x-axis. (c) Snapshot of normalized magnetization components of steady state domain wall for $J_{\rm RKKY} = -10.0$ meV at $J = 5 \times 10^{11}$ A/m^2. (d) Enlarged snapshot of M_y component corrsponding to (c). The frequency of emitted spin-waves is about 3.2 THz.

current threshod, resulting in THz spin-wave emission. On the other hand, in case of synthetic antiferromagnets with weak(reasonable)-to-intermediate $J_{\rm RKKY}$, $v_{\rm DW}$ is unable to reach $v_{\rm max}$ because it saturates due to the domain wall angle tilting.

Therefore, the key factor to differentiate domain wall dynamics between *true* antiferromagnets and synthetic antiferromagnets is the strength of antiferromagnetic exchange which affects the domain wall angle tilting. In other words, for SOT-driven domain wall dynamics, the damping-like SOT tilts the domain wall angle whereas the antiferromagnetic exchange suppresses such tilting. In case of *true* antiferromagnets, the antiferromagnetic exchange is very strong (i.e., $A_{\rm sim} = 16.0$ meV for the results shown in the main text) so that the domain wall angle does not tilt almost at all. Even in case of synthetic antiferromagnets, the RKKY antiferromagnetic exchange suppresses the domain wall angle tilting but its suppression is considerably weaker than that of *true* antiferromagnets. As a result, for $J_{\rm RKKY} = -1.0$ and -5.0 meV, the domain wall angle tilting is not sufficiently suppressed and $v_{\rm DW}$ saturates without any spin-wave emission. On the other hand, for a larger RKKY coupling ($J_{\rm RKKY} = -10.0$ meV), we find that $v_{\rm DW}$ (domain wall angle) is larger (smaller) than the other two cases and small-amplitude spin-waves are emitted at a large current density ($J = 5 \times 10^{11}$ A/m^2 shown in Fig. 2(c) and (d)), which is consistent with our understanding based on the strength of antiferromagnetic exchange.

To summarize, synthethic antiferromagents show SOT-driven domain wall dynamics similar to *true* antiferromagnets. However, THz spin-wave emission may be not possible for synthetic antiferromagnets with a reasonable $J_{\rm RKKY}$ (i.e., $J_{\rm RKKY} = -1.0$ meV) because the antiferromagnetic exchange is insufficient to suppress the domain wall angle tilting. Therefore, we conclude that THz spin-wave emission is unique to antiferromagnets when reasonable material properties are considered.

---

* These two authors contributed equally to this work.

† Electronic address: bgpark@kaist.ac.kr
‡ Electronic address: kj_lee@korea.ac.kr

[1] R. Cheng, J. Xiao, Q. Niu, and A. Brataas, Phys. Rev. Lett. **113**, 057601 (2014).
[2] R. Cheng, D. Xiao, and A. Brataas, Phys. Rev. Lett. **116**, 207603 (2016).
[3] S.-H. Yang, K.-S. Ryu, and S. Parkin, Nat. Nanotechnol. **10**, 221 (2015).